Bubble polarization domain patterns in periodically ordered epitaxial ferroelectric nanodot arrays

X. S. Gao,[1,2,a)] F. Xue,[3] M. H. Qin,[1] J. M. Liu,[3] B. J. Rodriguez,[2,4] L. F. Liu,[2] M. Alexe,[2] and D. Hesse[2]

[1]*Institute for Advanced Materials, School of Physics and Telecommunications Engineering, South China Normal University, 510006, People's Republic of China*
[2]*Max Planck Institute of Microstructure Physics, Weinberg 2, Halle D-06120, Germany*
[3]*Laboratory of Solid State Microstructures, Nanjing University, Nanjing 210093, People's Republic of China*
[4]*Conway Institute of Biomolecular and Biomedical Research, University College Dublin, Belfield, Dublin 4, Ireland*

(Received 8 February 2011; accepted 14 May 2011; published online 2 September 2011)

In this work, bubble polarization domains in periodically ordered ferroelectric $Pb(Zr_{0.4}Ti_{0.6})O_3$ nanodot arrays and their formation mechanisms have been investigated by piezoresponse force microscopy (PFM) and Monte-Carlo simulations. The PFM observations reveal the coexistence of single domain and apparent bubble domain patterns within the same nanodot array, which also exhibit dissimilar polarization reversal processes. The formation of various polarization configurations can be accounted for by the interplay of various factors, such as polarization anisotropy and depolarization field. Using Monte-Carlo simulation, we are able to reproduce bubble and single domains and further predict that these patterns can be tailored by varying the nanodot parameters, including dot height, aspect ratio, etc. © *2011 American Institute of Physics*. [doi:10.1063/1.3623766]

I. INTRODUCTION

In recent years, there has been a surge of research interests for nanoscale ferroelectrics driven by their potential for new generations of sensors and memories, especially for ultrahigh density data storage.[1,2] Memories based on ferroelectrics would enable nondestructive resistive readout and should be scalable down to a size of a few nanometers, thus overcoming the density limitation in current magnetic storage media. In addition, advanced fabrication techniques of both the "bottom-up" and "top-down" types have enabled fabricating extremely small high-quality epitaxial ferroelectric nanodots up to a few tens of nanometers in diameter and/or height.[3–6] The recent emergence of observation methods, such as piezoresponse force microscopy (PFM), has also given opportunities to observe local domain structures with sub-10 nm or even higher resolution.[7–10] In spite of these advances, there are still very few experimental investigations on the nanoscale polarization patterns compared with numerous theoretical studies.[11–13] Although a few polarization patterns, like vortex-like polarization, have been reported in thin films,[14,15] nanocapacitors,[16] stand-alone nanodots,[17] and nanodot arrays,[18] other possible patterns, like bubble domains or more complex polarization structures analog to those observed in nanomagnets, have rarely been addressed.

A core polarization state may be an indication of a vortex domain,[12] and evidence for such domain states have been presented,[18] wherein it was necessary to use both vertical piezoforce microscopy (VPFM) and lateral piezoforce microscopy (LPFM) to develop a full picture of the polarization state of the nanodot. It may be possible for certain conditions (size, strain, etc.) that a core polarization state is just a bubble domain with relatively small in-plane polarization compared with out-of-plane polarization. Here, we consider the latter case, based on VPFM images on $Pb(Zr_{0.4}Ti_{0.6})O_3$ (PZT) nanodot array only. The in-plane polarization was not studied in this case.

Monte-Carlo simulations were performed to further understand whether and how bubble domains can be formed and to give guidelines for further experimental studies.

II. EXPERIMENTAL PROCEDURE AND SIMULATIONS

The fabrication process for the epitaxial nanodots has been described in detail elsewhere.[5,18,19] Briefly, porous anodized alumina (AAO) shallow masks with self-ordered arrays of nanopores with various sizes and pitches were prepared by a two-step anodization process, then transferred to a $SrTiO_3$ substrate coated with a conductive $SrRuO_3$ electrode, and subsequently, pulsed laser deposition (PLD) was used to deposit $Pb(Zr_{0.4}Ti_{0.6})O_3$ nanodots. The AAO mask was then removed and a periodically ordered nanodot array was obtained. Finally, the products were annealed at a high temperature to form epitaxial nanodots. The crystal structure was then characterized by XRD Φ scans and reciprocal space mapping using a Philips X'Pert MRD diffractometer. The microstructure was characterized by scanning electron microscopy (SEM). PFM imaging was performed using a commercially available atomic force microscope (AFM) (TM Microscopes, Auto-Probe CP Research) equipped with a lock-in amplifier (DSP7260, Signal Recovery) and a PtIr5-coated conducting AFM tip (ATEC-EFM, Nanosensors).

The Monte Carlo simulations were performed on a 3D lattice circular disk with a diameter ϕ and dot height h, both

[a)]Author to whom correspondence should be addressed. Electronic mail: gaoxingsen@gmail.com.

given in numbers of unit cells. The modeling and simulation procedure has been described in our previous papers.[20] In brief, we define a 3D lattice, in which an electric dipole $P(i) = (P_x, P_y, P_z)$ and a displacement vector $u(i) = (u_x, u_y, u_z)$ are assigned to each site, where x, y, and z are the coordinate axes, respectively, and i is the site coordinate. Thus, each site corresponds to a unit cell of a realistic ferroelectric lattice system. Based on this lattice, we are able to develop the Landau phenomenological model, describing a tetragonal FE lattice as transformed from its parent cubic lattice at high T. For each lattice site, the free energy can be described as: $F(i) = f(i)_{Lan} + f(i)_{grad} + f(i)_{dip} + f(i)_{elast} + f(i)_{es} + f(i)_{Elec}$, where the terms $f(i)_{Lan}$, $f(i)_{grad}$, $f(i)_{dip}$, $f(i)_{elast}$, $f(i)_{es}$, $f(i)_{Elec}$ are the Landau potential, gradient energy, dipole-dipole interaction, elastic energy, electrostrictive interaction, and static electric energy, respectively. For a ferroelectric lattice, these terms constitute a complete set of energy terms in the phenomenological theory of ferroelectricity. The total energy of the system is the summation over every lattice site i. The detailed presentation for each energy term can be found elsewhere,[20] and the coefficients of the Landau free energy expansion and the electrostrictive and elastic constants for $Pb(Zr_{0.4}Ti_{0.6})O_3$ were adapted from the literatures.[21,22] We employ the Metropolis algorithm for the simulation,[20,23,24] starting from a lattice either with randomly distributed $P(i)$ and $u(i)$ or from single domain uniform polarization. We start from a randomly chosen site i, then update the value of P and u by a standard Metropolis procedure for the relaxation of electric dipole and elastic strain in the lattice. Given a fixed T, we perform the simulation for about 10^6 Monte Carlo steps (MCS) and then evaluate the domain structure and electrostrain.

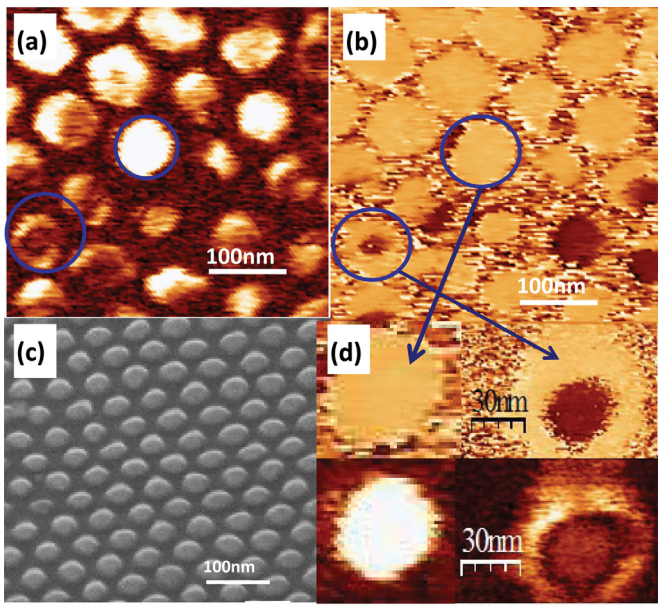

FIG. 1. (Color online) Piezoresponse force microscopy (PFM) and SEM images for the PZT nanodot array with different polarization domain patterns within the same nanodot array: out-of plane vertical PFM amplitude (a) and phase (b) micrographs; SEM image for the nanodots (c); magnified phase (upper) and amplitude (lower) images for both single polarization and bubble polarization domain states (d).

III. RESULTS AND DISCUSSION

Figure 1 shows an SEM micrograph as well as PFM amplitude and phase images for the as-fabricated PZT nanoisland array. Some nanodots show a uniform single-domain structure with a high piezoresponse signal, while other dots exhibit bi-domain or multidomain structures with a dark-bright contrast within a single nanodot (Figs. 1(a) and 1(b)). From the larger magnified images of the bi-domain dots (Fig. 1(d)), we can easily identify apparent ring-shaped bubble domains, wherein the outer diameter of the dot corresponds to a positively polarized domain (bright contrast in the phase image), while the inner portion is negatively polarized (dark). Bi-domain states, consisting of two oppositely polarized coaxial cylindrical domains, have been reported in some magnetic nanodisks with large perpendicular anisotropy and demagnetization. It was demonstrated that, inside the nanomagnets, the competition between the exchange energy, lattice anisotropy, and shape anisotropy leads to various domain configurations, like bubble or stripe domains.[25,26] In our epitaxial PZT nanodots on $SrTiO_3$ substrate, a large perpendicular anisotropy is expected, due to the compressive lattice misfit strain from substrate clamping, giving rise to c-axis polarization. On the other hand, PZT dots without top electrodes imply a large depolarization field. The competition between anisotropy and depolarization may lead to various domain structures as, e.g., a single domain in the anisotropy-dominant case, while it tends to lose stability and evolve into a more complex domain pattern in the depolarization-dominant case. We have also studied the lateral piezoresponse (not shown) and found that the lateral PFM images of those nanodots, which show apparent bubble domains in the vertical PFM images, also exhibit various patterns like single domains, ring shape, multidomains, or even the signature of vortex-like domains, as reported in our previous work.[18] As all these states have a up-down bubble domain along the vertical direction, for simplicity, we only consider here the vertical component in this stage. A 3D reconstruction of the complex domain states shall be the subject of future work.

Monte-Carlo simulations were performed using the Landau potential, gradient energy term, dipole-dipole interaction, elastic energy, and electrostrictive interaction. In these simulations, a large compressive misfit strain of –1% was applied, giving rise to strong c-axis anisotropy. Open-circuit boundary conditions were assumed, so that no screening charges are taken into consideration and a considerably large depolarization field can be expected. Although the model may be oversimplified and the geometric parameters used in the simulation are much smaller than those of the real nanodots, the simulation can still give qualitative comparisons between the theoretical predictions and the experimental observations. From our results, the domain states can be successfully reproduced by our Monte Carlo simulation. As shown in Fig. 2(a), at a small diameter (diameter $\phi = 15$ unit cells, dot height $h = 13$ unit cells, with a lattice unit of 0.4 nm), the nanodot is in a single-domain state with a slight variation in polarization, due to thermal fluctuations. With increasing dot size ($\phi = 33$, $h = 13$), the single domain

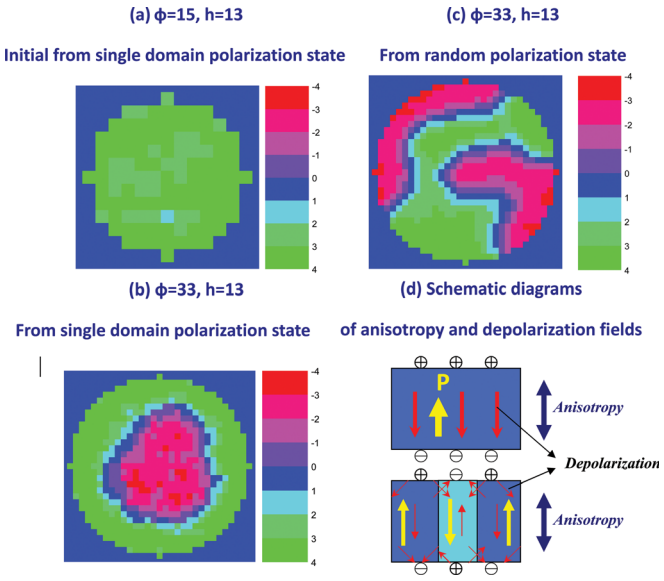

FIG. 2. (Color online) Monte-Carlo simulation micrographs of the z-component polarization distribution on the *z*-plane of the PZT nanodots as a function of diameter and initial states: (a) for the nanodot with small diameter of $\phi = 15$ and dot height of $h = 13$ unit cells (1 unit cell = 0.4 nm), (b) for the nanodot with $\phi = 33$ and $h = 13$, starting from a uniform polarization single domain state, and (c) for the nanodot with $\phi = 33$ and $h = 13$, starting from a random polarization state. The simulation was conducted under a compressive strain of –1%, and the snapshot micrographs were taken by averaging the polarization value along the vertical direction. The z-component polarization amplitude and phase were reflected by different colors (red (or dark contrast in print version): negative z-component polarization; green (or bright contrast in print version): positive z-component polarization). (d) Schematic diagrams for both single domain and multidomain nanodots subjected to the effects of depolarization and anisotropy, where the depolarization in single domain is rather strong and anti-domain develops to reduce the local depolarization field.

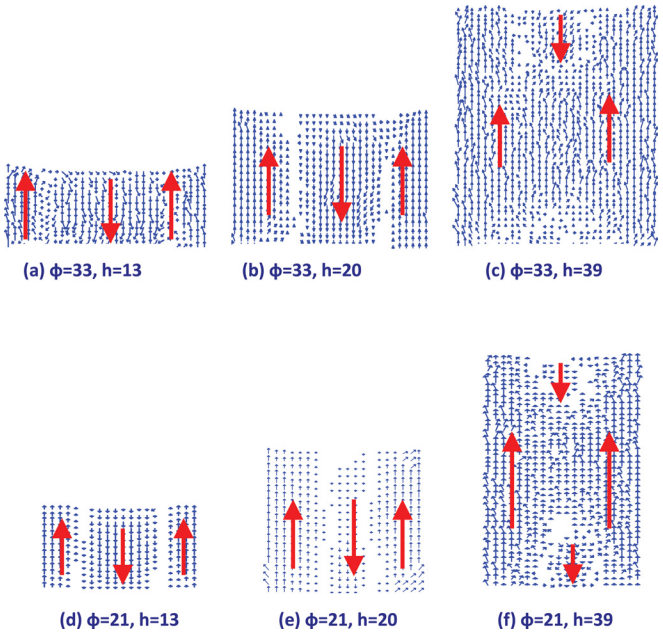

FIG. 3. (Color online) Simulated polarization distribution along the cross-section of a center vertical plane for the PZT nanodots: (a)-(c) demonstrate the evolution of polarization configuration as a function of dot height when fixing the diameter at $\phi = 33$; (d)-(f) show the evolution of polarization configuration with increasing dot height when fixing the diameter at $\phi = 21$. The blue small arrows indicate the orientation of the dipoles and red big arrows show the polarization direction of micro-domains.

becomes unstable and develops into a bubble domain, in which the inner core and outer ring have opposite polarizations, as shown by the different color contrast in the simulated micrograph (Fig. 2(b)).

Apparently, the domain pattern is considerably dependent on size and shape of the ferroelectric dot when the particle size goes into nanoscale, suggesting that the depolarization field plays an essential role in the refined system. At certain diameter and thickness, an anti-domain appears at the center of the nanodot, which lowers the depolarization energy. Further increases in the dot diameter adds to depolarization effect, resulting in an even more complex bubble domain state, e.g., a multiple bubble domain. Interestingly, if we start the simulation from an initially random state using the same parameters, a stripe like domain, instead of a bubble domain, can be obtained (Fig. 2(c)). The total energy difference between the stripe domain and bubble domain is very small, and the final state is very sensitive to the initial state. From our experimental observations, apparent bubble domains are far more abundant than stripe domains, implying that the pattern is more likely originating from a single domain initial state. The effects of depolarization and anisotropy have been schematically demonstrated in Fig. 2(d), in which the anisotropy field forces the polarization aligned along a perpendicular orientation. Without depolarization, single domain is the energetic favorable state, while the presence of depolarization tends to induce multi-domain to lower the total energy. As depolarization is very sensitive to geometric parameters of nanodots, various domain states can be obtained by simply adjusting the lateral size and vertical length. To examine the effect of depolarization field, we intentionally added a top electrode, covering the dots to screen the charge; the complex domain structure disappears (not shown here), further confirming the essential role of depolarization.

The simulation also reveals that the domain pattern is greatly dependent on the height of the nanodots, as illustrated by the evolution of the simulated polarization patterns as a function of dot height (Fig. 3). When fixing the dot diameter at $\phi = 33$ (Figs. 3(a)–3(c)), bubble domains occur in thin nanodots ($h = 13$ unit cell, around 5 nm). With increasing dot height, the fraction of core polarization domain becomes smaller and smaller. At a large height ($h = 39$), the core polarization domain almost disappears, leaving only small portions of edge anti-domains and the whole nanodot behaves more or less like a single domain. We also studied the thickness dependent effect for the dots with a smaller diameter ($\phi = 21$), as shown in Figs. 3(d)–3(f). A similar evolution trend can also be identified, although the portion of the core domain becomes smaller compared with dots with larger diameters. The above evolution trend can also be explained by the competition among depolarization field, anisotropy, and other intrinsic polarization coupling factors. For thinner dots, the depolarization field is dominant and the dots tend to have bubble domains to lower the depolarization energy, while the anisotropy and other couplings become significant for thicker dots, leading to a single domain-like polarization pattern.

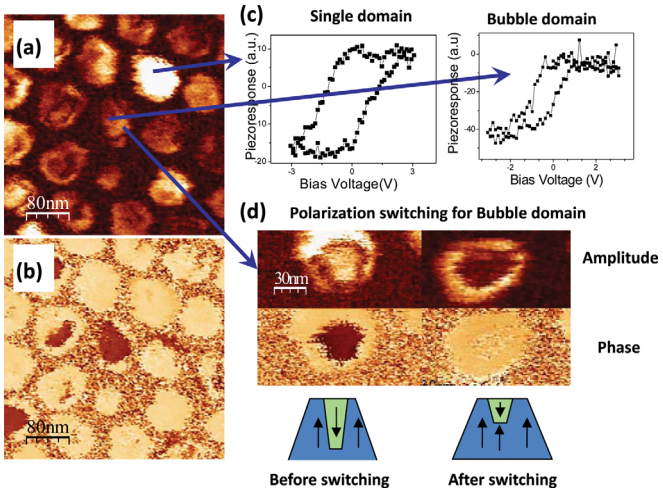

FIG. 4. (Color online) Polarization switching behavior for both a single and bubble domain state within the same PZT nanodot array: (a) and (b) out-of-plane vertical PFM amplitude and phase for the nanodot with both single domain state and bubble states, (c) piezoresponse hysteresis loop for the corresponding single domain state and bubble states, and (d) the amplified and phase images for the bubble domain before and after polarization reversal by applying an electric field through the AFM tip. The insets show schematic diagrams for the incomplete polarization reversal for the inner core domain.

As demonstrated above, the final polarization state depends on the geometric parameters of the nanodot, like diameter and height, which may explain the coexistence of various domain patterns (e.g., single domain, multidomain, vortex, etc.) inside the seemingly uniform nanodot array. From our previous studies, we observed a range of size distribution (e.g., 40-60 nm in diameter) within the same array, resulting from the fabrication process.[19] This indicates that the size variation could be the main reason for the inhomogeneous domain state. In addition, other possible factors, like strain nonuniformity and defects, can take effect. The above simulation also suggests a way to tailor the polarization domain patterns by precisely controlling size and shape of the nanodots.

Finally, we also inspected the domain switching behavior through PFM hysteresis loop measurements. Figures 4(a) and 4(b) show PFM amplitude and phase images for different domain states and their corresponding piezoelectric hysteresis loops. The single domain pattern shows a loop of more or less square shape, while the bubble domain exhibits a slim loop with large asymmetry, indicating different domain reversal processes (Fig. 4(c)). For dots with single domains, the polarization is more likely to show a uniform switching process, resulting in an approximate square loop. In contrast, the bubble domain shows a slimmer hysteresis loop, indicating a smaller coercive field. However, the hysteresis loop for the bubble domain is not symmetric, implying the presence of a non-switching region and a large imprint effect in the core polarization, probably due to the large depolarization field. This is further confirmed by the apparent contrast change in the domain pattern by applying an electric field from the AFM tip, as shown in Fig. 4(d). Before applying a field, the dot shows a bubble state with positive net polarization for the core and negative polarization for the outer ring. After applying a negative voltage, the phase contrast of the core polarization changes, indicating a switching of the polarization. However, the amplitude signal for the reversed bubble is rather weak, which implies that only part of the polarization domain is able to switch, while the rest of the portion remains unchanged, resulting in an overall small net polarization. In contrast, the single domain nanodot can be largely reversed after applying an electric field from the AFM tip (not shown here), in agreement with the relatively symmetric hysteresis loop. The above domain behavior and the switching dynamics will also be a subject of further studies that are required to obtain a deeper understanding of the domain evolution kinetics.

IV. CONCLUSIONS

In summary, bubble domains in periodically ordered ferroelectric nanodot arrays have been investigated both experimentally using PFM and theoretically by Monte-Carlo simulations. Vertical PFM shows a core-shell-like bubble domain structure, in which the ring edge and the inner core possess opposite polarizations. Monte-Carlo simulations show that different domain structures can be formed by adjusting the nanodot dimensions, e.g., dot height, aspect ratio, etc., through tuning the competition between anisotropy and depolarization energy. Thinner dots or large diameter ones are more likely to develop bubble domains, due to large depolarization energy, while nanodots with large height or dots with small lateral size tend to have a single-domain state, because, in this case, the anisotropy energy and other couplings become significant. The single domains and bubble domains also exhibit different polarization reversal processes, leading to dissimilar shapes of the PFM hysteresis loops.

ACKNOWLEDGMENTS

This work was supported by the Natural Science Foundation of China (Grant Nos. 51072061 and 51031004). Two authors X.S.G. and B.J.R. would also like to acknowledge the Alexander von Humboldt Foundation for financial assistance. J.M.L. also acknowledges the support from the 973 Project of China (Grant No. 2009CB923303).

[1]J. F. Scott, Science **315**, 954 (2007).
[2]J. F. Scott and C. A. Araujo, Science **246**, 1400 (1989).
[3]M. Alexe and D. Hesse, J. Mater. Sci. **41**, 1 (2006).
[4]S. K. Lee, W. Lee, M. Alexe, K. Nielsch, D. Hesse, and U. Gosele, Appl. Phys. Lett. **86**, 152906 (2005).
[5]W. Lee, H. Han, A. Lotnyk, M. A. Schubert, S. Senz, M. Alexe, D. Hesse, S. Baik, and U. Gosele, Nat. Nanotechnol. **3**, 402 (2008).
[6]W. Ma and D. Hesse, Appl. Phys. Lett. **84**, 2871 (2004).
[7]S. V. Kalinin, B. J. Rodriguez, S. Jesse, E. Karapetian, E. A. Eliseev, and A. N. Morozovska, Annu. Rev. Mater. Res. **37**, 189 (2007).
[8]S. V. Kalinin, B. J. Rodriguez, S. Jesse, J. Shin, A. P. Baddorf, P. Gupta, H. Jain, D. B. Williams, and A. Gruverman, Microsc. Microanal. **12**, 206 (2006).
[9]A. Gruverman, O. Auciello, and H. Tokumoto, Annu. Rev. Mater. Sci. **28**, 101 (1998).
[10]B. J. Rodriguez, S. Jesse, M. Alexe, and S. V. Kalinin, Adv. Mater. **20**, 109 (2008).
[11]I. I. Naumov, L. Bellaiche, and H. X. Fu, Nature **432**, 737 (2004).
[12]I. Naumov and A. M. Bratkovsky, Phys. Rev. Lett. **101**, 107601 (2008).
[13]J. Wang, Appl. Phys. Lett. **97**, 192901 (2010).

[14]S. K. Streiffer and D. D. Fong, MRS Bull. **34**, 832 (2009).
[15]Y. Ivry, D. P. Chu, J. F. Scott, and C. Durkan, Phys. Rev. Lett. **104**, 207602 (2010).
[16]A. Gruverman, D. Wu, H. J. Fan, I. Vrejoiu, M. Alexe, R. J. Harrison, and J. F. Scott, J. Phys.: Condens. Matter **20**, 342201 (2008).
[17]A. Schilling, D. Byrne, G. Catalan, K. G. Webber, Y. A. Genenko, G. S. Wu, J. F. Scott, and J. M. Gregg, Nano Lett. **9**, 3359 (2009).
[18]B. J. Rodriguez, X. S. Gao, L. F. Liu, W. Lee, I. I. Naumov, A. M. Bratkovsky, D. Hesse, and M. Alexe, Nano Lett. **9**, 1127 (2009).
[19]X. S. Gao, L. F. Liu, B. Birajdar, M. Ziese, W. Lee, M. Alexe, and D. Hesse, Adv. Funct. Mater. **19**, 3450 (2009).
[20]F. Xue, X. S. Gao, and J.-M. Liu, J. Appl. Phys. **106**, 114103 (2009).
[21]K. M. Rabe, C. H. Ahn, J.-M. Triscone, *Physics of Ferroelectrics: A Modern Perspective*, Topics in Physics (Springer-Verlag, Berlin, 2007), p. 363.
[22]M. J. Haun, Z. Q. Zhuang, E. Furman, S. J. Jang, and L. E. Cross, Ferroelectrics **99**, 45 (1989).
[23]Y. Cao, G. Sheng, J. X. Zhang, S. Choudhury, Y. L. Li, C. A. Randall, and L. Q. Chen, Appl. Phys. Lett. **97**, 252904 (2010).
[24]I. B. Misirlioglu, L. Pintilie, M. Alexe, and D. Hesse, J. Mater. Sci. **44**, 5354 (2009).
[25]M. Hehn, K. Ounadjela, J.-P. Bucher, F. Rousseaux, D. Decanini, B. Bartenlian, and C. Chappert, Science **272**, 1782 (1996).
[26]G. Hrkac, S. Bance, A. Goncharov, T. Schrefl, and D. Suess, J. Phys. D: Appl. Phys. **40**, 2695 (2007).